Supplementary Information

A Positron Emission Tomography Strategy for Visualizing Activated T Cells in Acute Graft-Versus-Host Disease

John A. Ronald[a,b,c,d*], Byung-Su Kim[e,*], Gayatri Gowrishankar[a,b], Mohammad Namavari[a,b], Israt S. Alam[a,b], Aloma D'Souza[a,b], Hidekazu Nishikii[e], Hui-Yen Chuang[a,f], Ohad Ilovich[a,b], Chih-Feng Lin[a,g,h], Robert Reeves[a,b], Adam Shuhendler[a,b], Aileen Hoehne[a,b], Carmel Chan[a,b], Jeanette Baker[e], Shahriar Yaghoubi[i], Henry F. VanBrocklin[j], Randall A. Hawkins[j], Benjamin L. Franc[j], Salma Jivan[j], James B. Slater[j], Emily F. Verdin[j], Kenneth T. Gao[j], Jonathan Benjamin[e], Robert S. Negrin[e], Sanjiv Sam Gambhir[a,b]

Supplementary Figures

Supplementary Figure 1

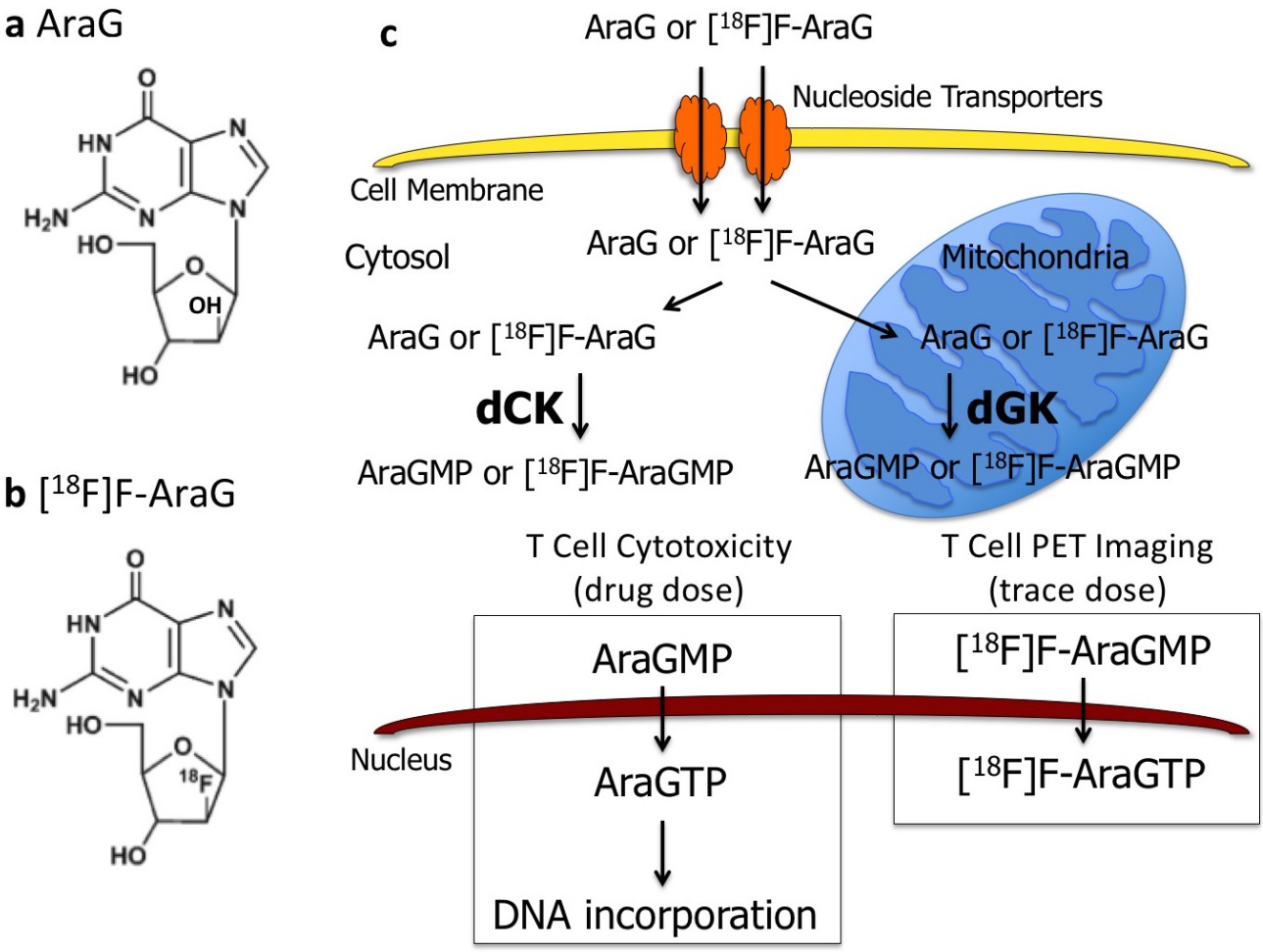

Supplementary Figure 1: [^{18}F]F-AraG Structure and Schematic of AraG Uptake into T Cells

a) Chemical structure of arabinofuranosyl guanine (AraG) **b)** Chemical structure of 2'-deoxy-2'-[^{18}F]fluoro-9-β-D-arabinofuranosyl guanine ([^{18}F]F-AraG). **c)** AraG, and putatively the radiotracer [^{18}F]F-AraG, are transported into cells via two nucleoside transporters, followed by the rate-limiting conversion to AraGMP or [^{18}F]F-AraGMP via phosphorylation by either cytosolic deoxycytidine kinase (dCK) or mitochondrial deoxyguanosine kinase (dGK). Further phosphorylation leads to AraGTP or [^{18}F]F-AraGTP formation. Bottom left: AraG given at drug doses, once converted to AraGTP, can outcompete deoxyGTP to be incorporated into DNA during cellular mitosis, leading to chain termination and triggering of the

apoptotic cascade in T cells. Bottom right: [^{18}F]F-AraG given at trace doses should not cause any pharmacological effects but its accumulation in activated T cells can be utilized to visualize these cells in PET imaging studies.

Supplementary Figure 2

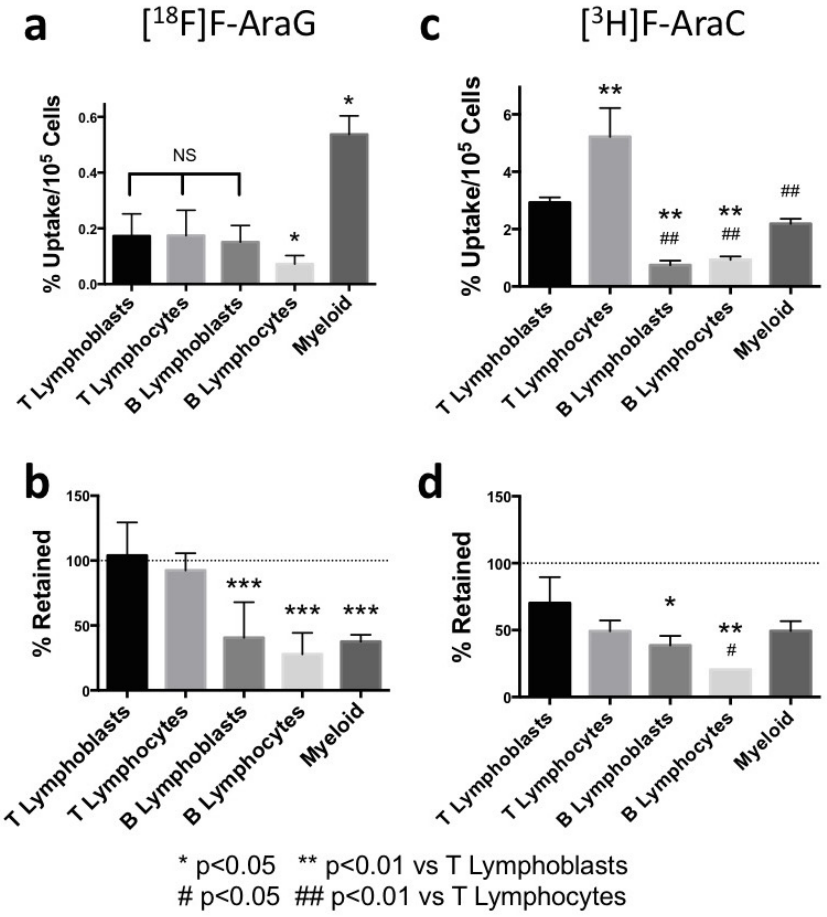

Supplementary Figure 2: [^{18}F]F-AraG and [^{3}H]F-AraC Uptake and Retention Across Various Immune Cell Lines

Uptake **(a)** and retention **(b)** of [^{18}F]F-AraG across several immune cell lines (n=9 per cell line; 3 replicates per experiment, experiment performed 3 times). Compared to all other cell lines, uptake was significantly higher and lower in myeloid cells and B lymphocytes respectively, (*p<0.05 versus T cell lines), but retention was significantly higher in T cell lines versus other immune cell lineages (***p<0.001 versus T cell lines). Uptake **(c)** and retention **(d)** of tritiated 1-(2'-deoxy-2'-[^{18}F]fluoro-D-

arabinofuranosyl) cytosine ([^{3}H]F-AraC) was investigated across several immune cell lines (n=3 for all cell lines). Compared to T lymphoblasts, significantly higher and lower tracer uptake in T lymphocytes and B cell lines was noted respectively (**p<0.01). Compared to T lymphocytes, significantly lower uptake was noted across all other cell lines (##p<0.01). Equivalent retention was revealed between T lymphoblast, T lymphocyte and myeloid cell lines. Significantly decreased retention was seen in B cells versus T lymphoblasts (*p<0.05, **p<0.01), as well as significantly decreased retention in B versus T lymphocytes (*p<0.05). Data in all graphs are expressed as mean ± SD.

Supplementary Figure 3

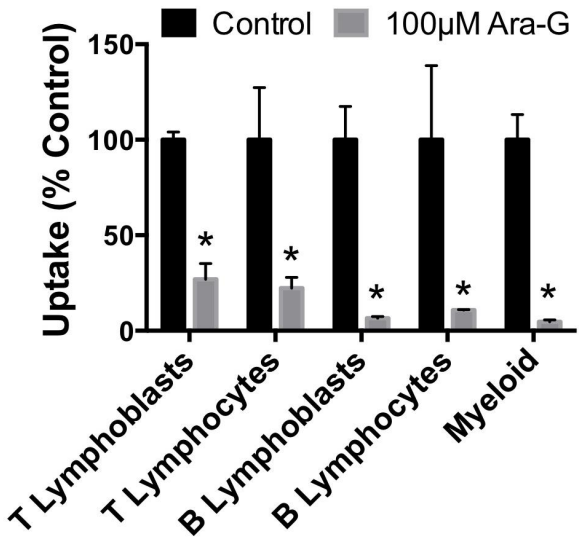

Supplementary Figure 3: AraG Competitive Inhibition of [^{18}F]F-AraG Uptake Across Various Immune Cell Lines.

Excess AraG (100 μM) was able to significantly (*p<0.05 versus control) inhibit uptake of [^{18}F]F-AraG in all cell lines (n=3 per cell line per treatment).

Supplementary Figure 4

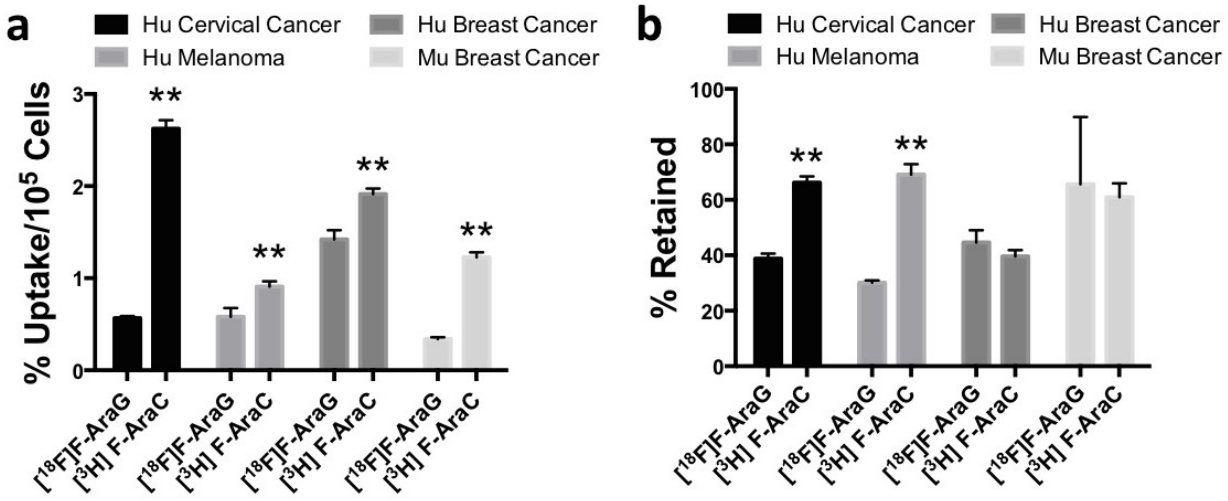

Supplementary Figure 4: Comparison of [^{18}F]F-AraG and [^{3}H]F-AraC Uptake and Retention Across Various Solid Tumor Cell Lines

Uptake **(a)** and retention **(b)** of [^{18}F]F-AraG and [^{3}H]F-AraC was investigated across several solid tumor cell lines (n=4 for per cell line per treatment). Significantly higher uptake was seen with [^{3}H]F-AraC versus [^{18}F]F-AraG for all cell lines (**p<0.01). In addition, significantly increased retention was seen in both human cervical cancer and melanoma cells with [^{3}H]F-AraC versus [^{18}F]F-AraG (**p<0.01). Data in all graphs are expressed as mean ± SD.

Supplementary Figure 5

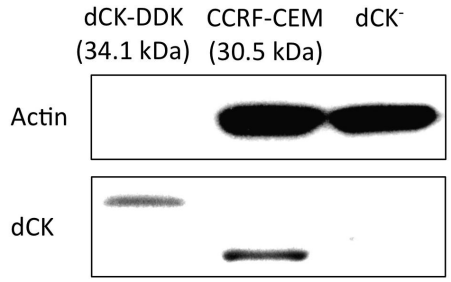

Supplementary Figure 5: Western Blot Analysis of dCK Expression in Wild-type and Mutant CCRF-CEM cells

dCK protein expression was detected in both lane 1 (recombinant dCK with DDK tag; 34.1 kDA) and lane 2 (CCRF-CEM lysates), but not in mutant dCK$^-$ cell lysates.

Supplemental Figure 6

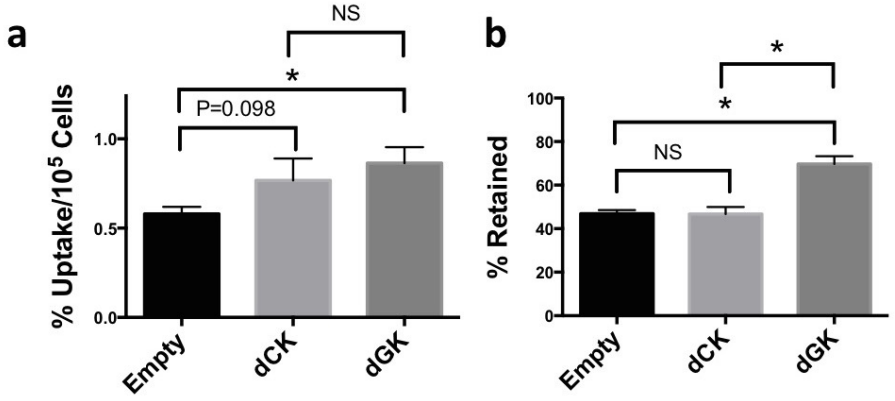

Supplementary Figure 6: dGK overexpression in CHO-K1 cells leads to increased [^{18}F]F-AraG uptake and retention.

Overexpression of mitochondrial deoxyguanosine kinase (dGK), but not cytosolic deoxycytidine kinase (dCK), in CHO-K1 cells lead to significantly higher uptake **(a)** and retention **(b)** of [^{18}F]F-AraG compared to empty vector treated cells (*$p<0.05$; n=3 per treatment).

Supplemental Figure 7

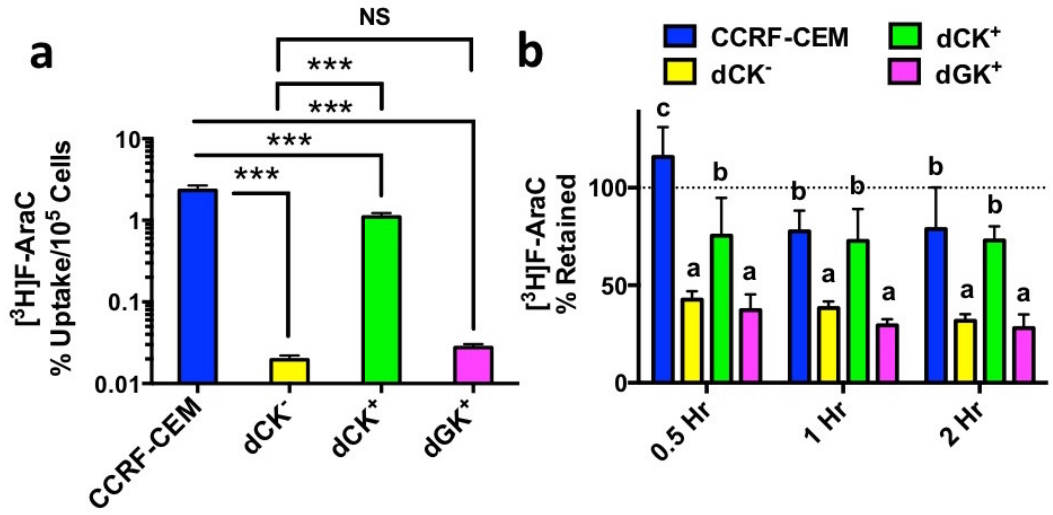

Supplementary Figure 7: [^{3}H]F-AraC Accumulates in Cells via dCK Activity

Uptake **(a)** and retention **(b)** of [^{3}H]F-AraC across wild-type CCRF-CEM T lymphoblasts, mutant CCRF-CEM dCK$^-$ cells (dCK$^-$), and dCK$^-$ cells overexpressing either dCK (dCK+) or dGK (dGK+) (n=4 per cell type per time point). Significantly less uptake was seen due to the loss of dCK in wild-type cells (***$p<0.001$; CCRF-CEM vs. dCK$^-$). Significantly higher uptake was found in dCK$^+$ versus dCK$^-$ cells (***$p<0.001$), but uptake in dCK+ cells was still significantly lower than wild-type cells (***$p<0.001$). dGK$^+$ cells had equivalent uptake compared to dCK$^-$ cells and significantly less than wild-type and dCK$^+$ cells (***$p<0.001$). Cells lacking dCK (dCK$^-$ and dGK$^+$) had significantly reduced ability to retain [^{3}H]F-AraC compared to wild-type and dCK$^+$ cells (different letters above bars represent significant differences between data sets at a nominal p-value of 0.05). Data in all graphs are expressed as mean ± SD.

Supplementary Figure 8

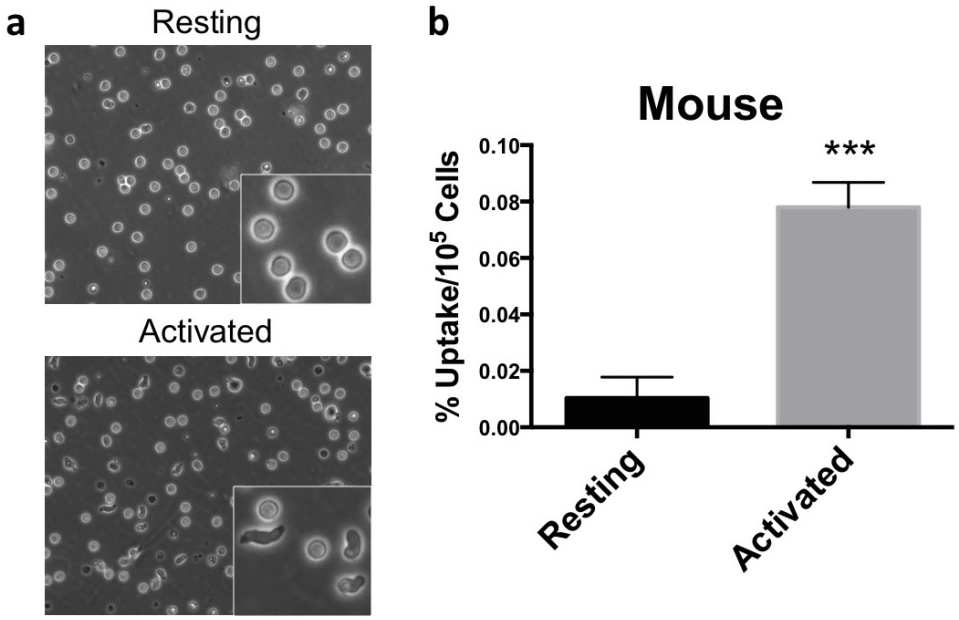

Supplementary Figure 8: Uptake of [^{18}F]F-AraG in Activated Versus Resting Murine T Cells

a) Activated (bottom) murine primary T cells displayed distinct morphological (elongated) characteristics compared to resting T cells (top). **b)** [^{18}F]F-AraG was taken up at significantly higher levels in activated versus resting cells (***$p<0.001$; n=3 per group).

Supplementary Figure 9

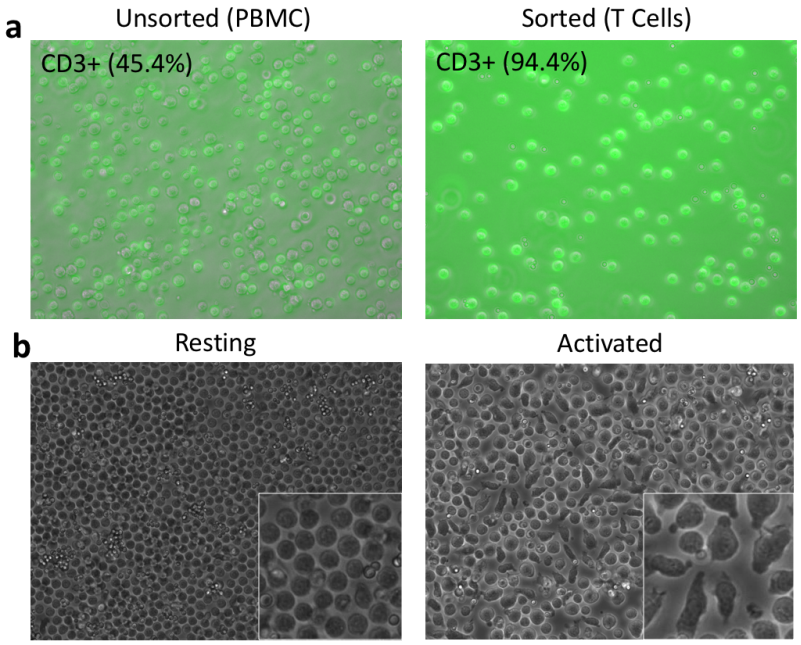

Supplementary Figure 9: Isolation and Activation of Primary Human T Cells

a) Negative-selection magnetic sorting of PBMCs yielded >90% CD3+ T cell population. **b)** Activated (right) human primary T cells displayed distinct morphological (elongated) characteristics compared to resting T cells (left).

Supplementary Figure 10

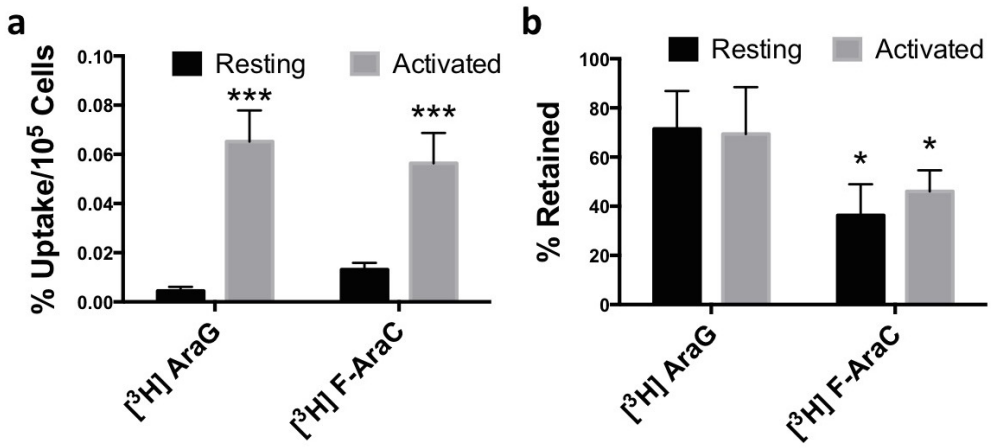

Supplementary Figure 10: Uptake and Retention of [^{3}H]AraG and [^{3}H]F-AraC in Resting and Activated Human Primary T Cells

Human primary T cells were isolated from PBMC buffy coats, activated in culture for 2 days, and incubated with either [^{3}H]AraG or [^{3}H]F-AraC to measure uptake **(a)** and retention **(b)**; n=3 per treatment per tracer). Both tracers were taken up at significantly higher levels (~6-7 fold) in activated versus resting T cells (***$p<0.001$). In contrast, [^{3}H]AraG was retained at significantly higher levels (~30% more) within both resting and activated T cells versus [^{3}H]F-AraC (*$p<0.05$). Data in all graphs are expressed as mean ± SD.

Supplementary Figure 11

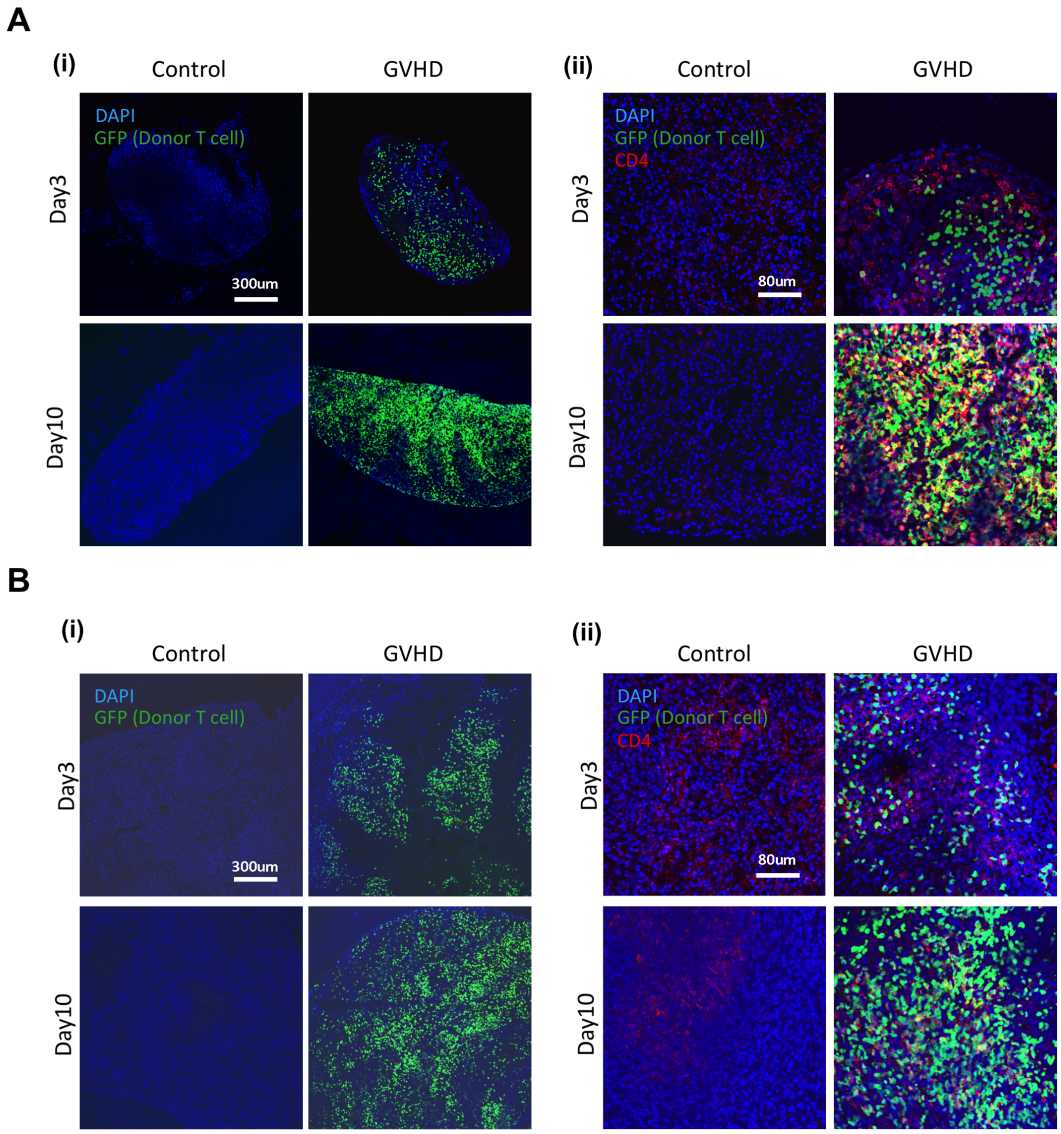

Supplementary Figure 11: Evaluation of GFP+ Donor T cells in Spleens and Cervical Lymph Nodes (CLNs) at Day 3 and Day 10 of Acute GVHD

Control (BM transplanted mice) and GVHD (GFP+T cells injected mice) mice were sacrificed at day 3 and day 10 after transplantation. (**A**) Cervical lymph nodes (CLNs) were harvested to evaluate the infiltration of GFP+ donor T cells by immunohistochemistry [(i): Green, GFP; Blue, DAPI; Scale bar, 300 μm]. The results of immunostaining with an anti-CD4 antibody are also shown [(ii): Green, GFP; Red, CD4; Blue, DAPI; Scale bar, 80 μm]. (**B**). Spleens were harvested and evaluated [(i): Green, GFP; Blue, DAPI; Scale bar,

300 μm]. The results of immunostaining with anti-CD4 antibody were also shown [(ii): Green, GFP; Red, CD4; Blue, DAPI; Scale bar, 80 μm]. Note that the frequencies of GFP+ donor T cells on day 10 were higher that those on day 3.

Supplementary Figure 12

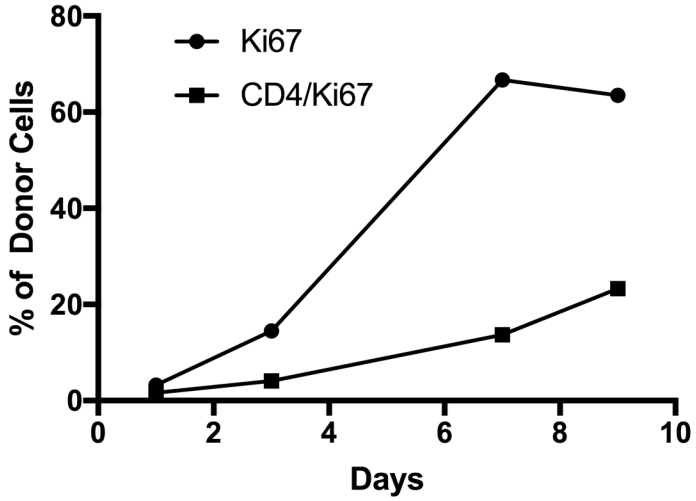

Supplementary Figure 12: Evaluation of Proliferation of Donor T Cells in Cervical Lymph Nodes

Cells from the cervical lymph nodes from 3 mice at each time point were pooled and analyzed by flow cytometry for the percentage of proliferating (Ki-67) donor T cells and $Ki67^{+}/CD4^{+}$ donor T cells at each time point. Higher percentages were noted at 7 and 9 days compared to days 1 and 3.

Supplementary Figure 13

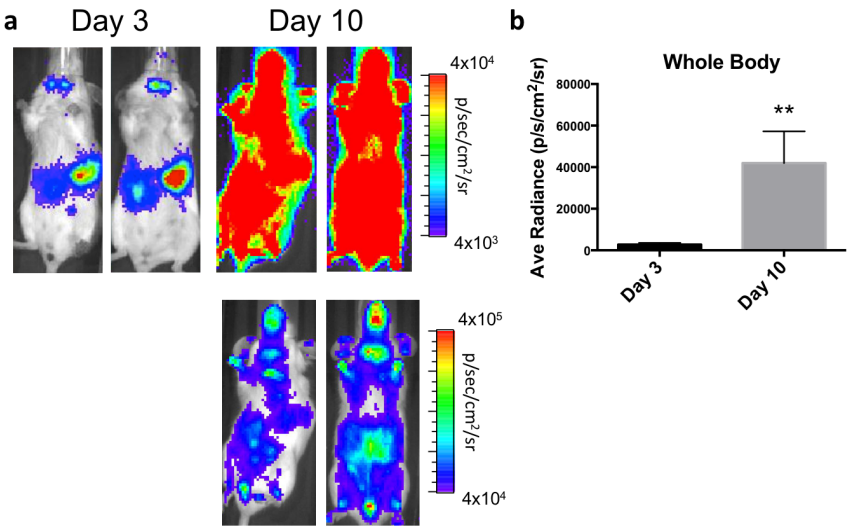

Supplementary Figure 13: BLI images of day 3 and day 10 GVHD mice.

a) Qualitatively, more BLI signal (i.e., more luciferase-expressing donor T cells) were detected at day 3 versus day 10 mice (upper images on the same image scale). At an order of magnitude higher image scale for the day 10 images (bottom images), one notes higher signal in the cervical lymph node region even compared to the same region at day 3 at the lower image scale. **b)** Significantly higher total body BLI signal was detectable on day 10 versus day 3 ($p<0,01$), highlighting the proliferation and dissemination of donor T cells as the disease progresses.

Supplementary Table 1: [^{18}F]F-AraG standard uptake values for key tissues- normalized to body weight (SUV-BW) at 47-77 minutes post tracer injection in six healthy human volunteers.

Site	SUV-BW $_{mean}$	SUV-BW $_{max}$
Brain Tissue	0.02 ±0.01	0.08±0.02
Cervical Lymph Node	5.2 ±1.15	7.13±1.76
Heart	2.12 ±0.72	4.72 ±1.37
Myocardium	3.38 ±1.19	4.72±1.37
Liver	13.47 ±1.46	16.18±2.00
Kidney (right)	20.72±5.26	44.47±12.44
Kidney (left)	17.27±4.19	41.35±10.65
Bladder	8.28 ±6.15	10.28± 7.66
Muscle	0.98 ±0.44	1.42±0.66

SUV-BW mean and max values shown. Data shown represent averages ± standard deviation; n=6 for each site. Average of both right and left sides of subject shown for following sites: brain tissue and cervical lymph node.

Supplementary Table 2: [^{18}F]F-AraG human radiation dosimetry data

Organs	Male	Female
Adrenals	0.046567	0.067133
Brain	0.006380	0.007407
Breasts	0.005757	0.007547
Gallbladder Wall	0.051400	0.063033
LLI Wall	0.085107	0.012150
Small Intestine	0.047033	0.073000
Stomach Wall	0.018667	0.025367
ULI Wall	0.022600	0.033067
Heart Wall	0.052533	0.096933
Kidneys	0.877000	1.133333
Liver	0.211000	0.266667
Lungs	0.027167	0.033133
Muscle	0.009190	0.012167
Ovaries		0.016967
Pancreas	0.037300	0.050200
Red Marrow	0.013600	0.016833
Osteogenic Cells	0.007390	0.010593
Skin	0.004543	0.005790
Spleen	0.093600	0.163667
Testes	0.002780	
Thymus	0.005710	0.007800
Thyroid	0.001357	0.001633
Urinary Bladder Wall	0.085800	0.088167
Uterus	0.014133	0.017500
Total Body	0.018767	0.025200
Effective Dose	0.0138 mSv/MBq	

Average mean radiation dosimetry data in 3 males and 3 females in REM/mCi. The kidneys receive the highest radiation dose followed by the liver.